

RESEARCH ARTICLE

Downscaling of seasonal ensemble forecasts to the convection-permitting scale over the Horn of Africa using the WRF model

Paolo Mori  | Thomas Schwitalla  | Markos Budusa Ware  |
Kirsten Warrach-Sagi  | Volker Wulfmeyer 

Institute for Physics and Meteorology,
University of Hohenheim, Stuttgart,
Germany

Correspondence

Paolo Mori, Hohenheim University,
Institute for Physics and Meteorology,
Garbenstraße 30, 70599 Stuttgart,
Germany.
Email: paolo.mori@uni-hohenheim.de

Funding information

High Performance Computing Center
Stuttgart (HLRS), Grant/Award Number:
WRFSFHOA/ACID 44111

Abstract

The new SEAS5 global ensemble forecast system was dynamically downscaled over the Horn of Africa for summer (June-July-August) 2018. For this purpose, a multi-physics ensemble was designed with a grid increment of 3 km and without any intermediate nest based on the Weather Research and Forecasting model (WRF). The WRF and the SEAS5 model output were compared with each other and reference datasets to assess the biases in 4 different regions of Ethiopia. Also, the WRF ensemble variability was investigated in relation to model parameterization and lateral boundary conditions. Over the summer, the SEAS5 has a positive temperature bias of 0.17°C compared to ECMWF analysis average for the study domain, while the WRF bias is +1.14°C. Concerning precipitation, the WRF model had average accumulated values of 264 mm, compared to 248 mm for SEAS5 and 236 mm for the observations. Over south Ethiopia, however, the downscaling produced over 50% more precipitation than the other datasets. The maximum northward extension of the tropical rain belt was reduced by about 2° in both models when compared to observations. Downscaling increased reliability for precipitation, correcting the SEAS5 underdispersion: ensemble spread for precipitation was increased by about 70% in the WRF ensemble in three of the four Ethiopian sub-regions, whereas the very dry Somali region remained unaffected. The WRF ensemble analysis revealed that the ensemble spread is mainly caused by the perturbed boundary conditions, as their effect is often 50% larger than the physics-induced variability in the mountainous part of Ethiopia for precipitation and temperature.

KEYWORDS

convection-permitting, downscaling, ensemble, Ethiopia, SEAS5, seasonal forecast, WRF

This is an open access article under the terms of the Creative Commons Attribution-NonCommercial License, which permits use, distribution and reproduction in any medium, provided the original work is properly cited and is not used for commercial purposes.

© 2020 The Authors *International Journal of Climatology* published by John Wiley & Sons Ltd on behalf of Royal Meteorological Society.

1 | INTRODUCTION

Accurate and reliable seasonal forecasts are fundamental tools for decision making in many sectors like agriculture, water management, and early warning systems (Feldman and Ingram, 2009). Advanced seasonal forecasts are becoming even more important considering the expected global warming and the related higher probability of extreme events, that is, heavy rainfall, floods, heatwaves and droughts (Min *et al.*, 2011; Osima *et al.*, 2018). Global seasonal forecasts are produced at NOAA (National oceanic and atmospheric administration), ECMWF (European Centre for Medium-Range Weather Forecasts), UK Met Office and other centres worldwide. Their results are collected and disseminated through the world meteorological organization. Improvements of seasonal simulations depend on two factors: on the one hand, progress in the understanding and modelling of processes related to long-term predictability in various regions of the world. Sources of predictability beyond a two-week period have been identified in sea surface temperature (SST) anomalies (Shukla, 1998), ice and snow cover (Cohen and Entekhabi, 1999), stratosphere-troposphere interactions (Thompson *et al.*, 2002), soil moisture (Koster *et al.*, 2004), and vegetation state (Tölle *et al.*, 2014). On the other hand, a larger amount of observations has progressively become available to initialize forecasts. Enhanced prediction skills were recently reported for tropical (Stockdale *et al.*, 2018) or extratropical 2-m temperature (Vitart, 2014), and the Madden-Julian Oscillation phases (Vitart, 2014). New model developments have reduced the monthly SST bias in the equatorial Pacific, the critical region for the El Niño Southern Oscillation (ENSO), by more than 1°C at lead times of two months and longer (Stockdale *et al.*, 2018). For the United Kingdom MetOffice GloSea5 model, the global correlation between ENSO phases and precipitation patterns saw a statistically significant increase from 0.76 to 0.80 from the previous model version (Maclachlan *et al.*, 2015).

However, at sub-seasonal and seasonal time scales the horizontal resolution of global prediction models is coarser than 10 km. As a cumulus scheme is necessary at this grid size to simulate convection, large uncertainties in precipitation amount and timing are introduced (Prein *et al.*, 2015). Coarse-resolution models underperform in regions with complex topography such as coastlines and mountain ranges (Schwitalla *et al.*, 2008; Prein *et al.*, 2013). High resolution is also important when modelling smaller water bodies like lakes and wetlands (Lauwaet *et al.*, 2012).

In order to achieve higher resolution it is possible to downscale a global model over the region of interest.

Smaller domains make the simulations affordable: regional climate models (RCM) at the convection-permitting (CP) scale have been a common research tool in the last decade (Prein *et al.*, 2015). The advantages of CP models for seasonal climate modelling are lower biases and better skill scores (Schwitalla *et al.*, 2017; Pal *et al.*, 2019).

Seasonal forecasts specifically for Ethiopia have been prepared since 1987: the Ethiopian National Meteorology Agency (NMA) began using the analogue method to classify years according to SSTs in the equatorial Pacific (El Niño index) and Indian Oceans. Seasonal forecasts for precipitation were issued based on the precipitation on record during the most similar years (Korecha and Sorteberg, 2013). More advanced statistical methods have been implemented by NMA, using Canonical Correlation Analysis (Fekadu, 2015). To improve the forecasts, studies assessing the impact of dynamically predicting the ENSO state were performed (Korecha and Barnston, 2007) but never included in the operational routine. Testing of suitable model configurations for seasonal predictions in Ethiopia began in 2015, at 30 km grid increment (Regassa, 2014). A collaboration between NMA and the United Kingdom MetOffice has recently been established through the UN Office for the Coordination of Humanitarian Affairs to provide seasonal forecasts based on state-of-the-art GCM (SCIPEA, 2019, consulted on November 27, 2019).

In the Horn of Africa, the intertropical convergence zone movement defines rainfall seasonality: south Ethiopia, Kenya and southern Somalia have a bimodal rainfall pattern with rainy periods in spring and autumn. The northern part is subjected to a unimodal rain distribution: depending on the position, the wet spell lasts up to 4 months (June to September), but it shortens moving to the north and to the east. In Section 2.3, we present four sub-regions, whose climatology illustrates the different seasonal cycles. Given that summer rainfall over the highlands is the fundamental water source for a region where most of the farmland consists of rain-fed agriculture (Korecha and Sorteberg, 2013), improvements in seasonal forecasts have strong practical benefits. However, even if some teleconnections and SST global-scale patterns have been found to explain summer rainfall variability (Fekadu, 2015; Gleixner *et al.*, 2017), global models have generally low skills in forecasting summer precipitation anomalies over the Horn of Africa (Batté and Déqué, 2011; Nikulin *et al.*, 2018). A multi-model downscaling effort was carried out as part of the EUPORIAS project for Ethiopia, using atmospheric hindcasts and SSTs from reanalysis to force a 25 km resolution RCM but the results showed only limited skill improvement concerning the summer rains (Nikulin *et al.*, 2018).

Overall, few works on dynamical downscaling of ensemble seasonal forecasts (or hindcasts) have been published (Díez *et al.*, 2011; Castro *et al.*, 2012; Diro *et al.*, 2012; Yuan *et al.*, 2012; Siegmund *et al.*, 2015; Cheneka *et al.*, 2016; Diro, 2016; Nikulin *et al.*, 2018); only Siegmund *et al.* (2015) used a grid increment finer than 25 km, namely 10 km.

Of the seasonal downscaling studies Nikulin *et al.* (2018) included simulations performed with the Weather Research and Forecasting (WRF) model (Skamarock *et al.*, 2008) versions 3.4.1 and 3.8.1. It is interesting to note that, while the two configurations performed similarly elsewhere, the newer version has much higher inter-annual correlation with precipitation observation over the central Ethiopian highlands than its older counterpart. Recent WRF simulations in East Africa include a model configuration test for operational applications by NMA (Regassa, 2014) with a 30 km grid to test WRF land-surface model sensitivity. To investigate land-cover and resolution effects in the Tana Basin, Kerandi *et al.* (2017) used WRF at 25 and 50 km, concluding that higher resolution benefits rainfall simulation. In preparation for climate runs, Argent *et al.* (2015) tested the WRF ability on a 10 km grid to represent the rainfall patterns around the Victoria Lake, including several physics schemes. The most complete study on WRF sensitivity in East Africa was conducted by Pohl *et al.* (2011), using WRF3.1. They included physics parameterization, domain size, land-surface model, land-use, lateral boundary conditions (LBCs) and number of vertical levels. When comparing several climate model at 50 km resolution, WRF simulates the highest amount of precipitation in East Africa (Endris *et al.*, 2013). The new ECMWF SEAS5 ensemble for global seasonal forecast is operational since 2018, and due to the increased resolution of 0.3° (~36 km at the equator) it is possible to force a convection-permitting RCM without any intermediate nested domains using a cumulus scheme.

This work has two goals: firstly, we want to investigate the possible improvements in temperature and precipitation values through downscaling the new seasonal forecasts at the CP scale over the Horn of Africa, which is a very promising testing ground. Secondly, we aim to quantify the relative influence of physics and boundary condition perturbations on the model output. This allows us to assess the largest source of uncertainty once the cumulus scheme is removed. For ensemble forecasts it is important to know how much spread can be generated in a limited-area model (LAM), whereas for regional modelling it is useful to understand the relative uncertainty magnitude.

The following scenario was prepared: using the WRF 3.8.1 model, a multi-physics ensemble was initialized and

forced using four SEAS5 ensemble members, on a limited-area domain, to downscale the forecast for June–July–August (JJA) 2018.

The paper is structured as follows: in Section 2 the experimental set-up, including reference datasets and the ensemble composition, is described. In Section 3 the convection-permitting ensemble biases and reliability for 2-m temperature (T2m) and precipitation are assessed and the effects of model settings on the ensemble spread are evaluated. In Section 4 we discuss the results. Conclusions and outlook are presented in Section 5.

2 | DATASETS AND METHODS

2.1 | Experimental set-up

The WRF-ARW model 3.8.1 was used to downscale the SEAS5 global seasonal ensemble forecasts for summer 2018.

2.1.1 | ECMWF SEAS5: Initial conditions and boundary forcing

The SEAS5 seasonal ensemble forecast was used to force the LAM at the boundaries.

The ECMWF system has a T319 spectral horizontal resolution for model dynamics and a O320 Gaussian grid for the physical parameterization, which corresponds to an approximate resolution of 36 km. A global simulation of 7 months is initialized at the first day of each month using operational analysis for the atmosphere and the land-surface variables. The “Nucleus for European modelling of the ocean” (NEMO) model is initialized using the operational sea-surface temperature and sea-ice analysis (OSTIA) real-time product and initial conditions are perturbed to obtain a 5-member ensemble. This is then extended to a 51-members ensemble including the atmospheric model perturbations. Further details are given in Johnson *et al.* (2019).

Due to storage constraints, only a small sub-set of vertical model levels is available for the downscaling: half of them (46 of 91), and for 11 out of 51 ensemble members. Lateral boundary conditions and SST for the downscaling were prepared using the control run (member 0) and 3 perturbed members (members 1, 2, and 3) of the SEAS5 ensemble. The perturbed members 1, 2, and 3 saw less abundant precipitation than the control in the summer months and they have very similar mean temperature. Together with the control run, they provided a good representation of the ensemble spread for SSTs and atmospheric fields (not shown).

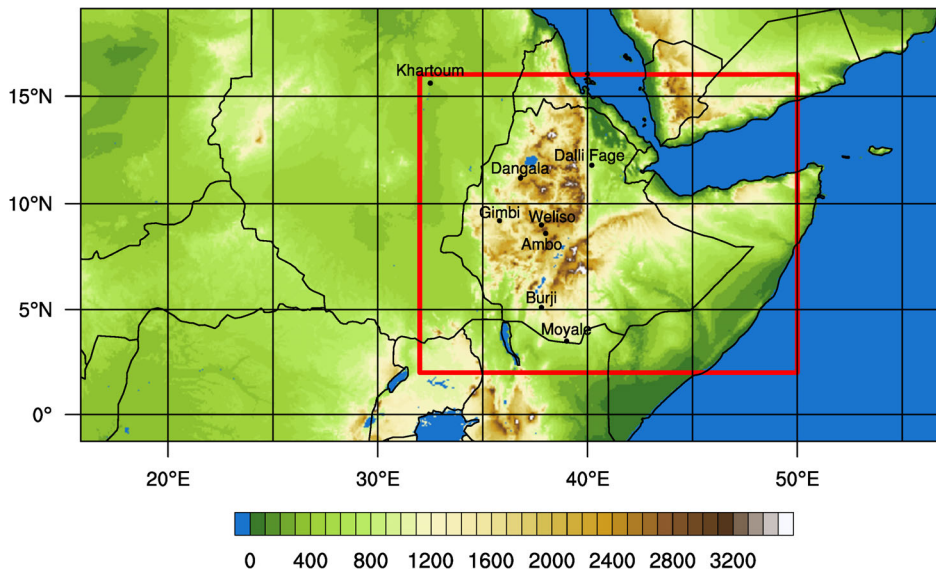


FIGURE 1 WRF model topography at 3 km resolution. The study area is depicted in the red box. Weather stations are marked by black dots [Colour figure can be viewed at wileyonlinelibrary.com]

Since the SEAS5 system has been operational since December 2017, only 1 year of data archived on model levels was available for downscaling. Vertical pressure level only are provided for re-forecasts, which are insufficient for dynamical downscaling.

2.1.2 | The WRF model

WRF is a community numerical weather prediction model with many available parameterizations for atmosphere and land-surface physics, suitable for sensitivity tests. The chosen land-surface model NOAH-MP has been developed with the purpose to facilitate climate predictions with physically-based ensembles (Niu, 2011). However, the land-surface model perturbation in a multi-physics ensemble is left for future work.

The LAM (Figure 1) was centred over the Ethiopian highlands and the Horn of Africa. One of the main concerns was to account for the spatial spin-up of the low-level westerly winds flowing in from the Atlantic Ocean because of their crucial role in transporting moisture to the region in summer. Therefore, the western boundary of the domain was kept far apart from the region of interest, reducing numerical artefacts that would degrade the simulation.

The grid increment was 3 km with 56 vertical levels up to 10 hPa. The model domain consisted of $1500 \times 750 \times 56$ grid points. The resolution jump was higher than the optimal ratio but it was considered acceptable in past RCM studies (Denis *et al.*, 2003; Antic *et al.*, 2004).

LBCs were interpolated by the WRF preprocessing system and updated every 6 hr. The lower boundary was

updated every 24 hours. The land-use data were derived from IGBP-Modified MODIS and the standard WRF soil categories were used.

To give the LAM a sufficient spin-up time from a cold start, the forecast initialized on the first of March 2018 was used to investigate summer (JJA) of 2018.

2.1.3 | The ensemble set-up

The ensemble was designed to compare the effects of boundary conditions and parameterizations on the LAM uncertainties. In the following, ensemble spread is interpreted as the perturbation effects on model output. Initial terrestrial lower boundary conditions have little to no impact on the forecast as the spin-up time is longer than the soil-moisture memory. Therefore only SSTs and lateral boundaries matter in practice, involving the 3D atmospheric fields. For consistency, only changes of atmospheric parameterization are considered, and we omitted land-surface perturbations in this experiment. Once the cumulus scheme is turned off, the other relevant atmospheric physics schemes are: short-wave (SW) radiation scheme, surface layer and planetary boundary layer (PBL), and microphysics (MP) (Pohl *et al.*, 2011).

Parameterization uncertainties affect the atmospheric model and precipitation is especially sensitive to model configuration. Next we describe the characteristics of the physics schemes included in the multi-physics ensemble.

The total amount of energy available at the surface skin is the fundamental starting point to simulate all atmospheric processes. Therefore, the incoming SW radiation influences skin temperature, the consequent

partition of energy into sensible heat and latent heat fluxes, outgoing long-wave radiation, and turbulence, with various consequences on temperature and precipitation patterns. One large source of uncertainty is the interaction of radiation with hydrometeors: the community atmospheric mode (CAM) scheme simulates radiation interactions with three hydrometeors types: cloud water, cloud ice and snow (Collins *et al.*, 2004), whereas the Rapid radiative transfer model for GCMs (RRTMG) adds the interaction with rain (Iacono *et al.*, 2008).

The PBL scheme deals with energy, moisture and momentum fluxes near the Earth's surface, where turbulent mixing is responsible for thermodynamic and kinematic profiles. The transport of moisture and heat through the boundary layer is a key factor for initiation of convection and cloud development. A local scheme and a non-local one were used to address the differences in the turbulence parameterization. YSU is a non-local scheme that treats the turbulence by a first order closure (Hong *et al.*, 2006). On the contrary, MYNN is a local scheme based on the Mellor-Yamada parameterization and a Turbulent Kinetic Energy closure of order 2.5 (Nakanishi and Niino, 2009). The surface scheme is an independent source of uncertainty as it deals with the exchange of heat, moisture and momentum between the land-surface model and the PBL. However, for technical reasons, it cannot always be changed independently from the PBL. In this specific case, we chose to couple the PBL with the suitable surface schemes, namely the MM5 surface scheme for YSU and the MYNN surface scheme for the MYNN PBL parameterization.

Microphysics schemes deal with phase transitions and phenomena related to hydrometeors, like collision and coalescence. Approximations in the parameterization have strong consequences on rainfall timing, intensity, and duration. The complex relationships between the water phases in a cloud are not yet completely understood, therefore there is a large variety of microphysics schemes using different approaches. The Thompson scheme defines five hydrometeor classes: cloud water, cloud ice, rain, snow and graupel, having rain and cloud-ice double-moment schemes (Thompson *et al.*, 2008). Morrison 2-moments uses the same classification but the explicit treatment of hydrometeors' mass and number variables is expanded to four types, namely cloud ice, rain, graupel, and snow (Morrison and Gettelman, 2008). In case of deep convection, the Thompson scheme tends to produce higher cooling at and below the cloud base, reducing the convection strength and the cell lifetime with respect to Morrison. The latter shows a second peak in convective activity after about 1 hr from the convection initiation (Heikenfeld *et al.*, 2019): this potentially results in more intense convective precipitation when the Morrison parameterization is used.

TABLE 1 Physics schemes included in the WRF ensemble: control member in the central column, alternative parameterization on the right

Physics parameterization	Control member	Ensemble variation
Planetary boundary layer (surface scheme)	MYNN (MYNN)	YSU (MM5)
Microphysics	Morrison 2-mom	Thompson
Short-wave radiation	RRTMG	CAM

The RRTMG scheme for short-wave radiation, the MYNN PBL scheme and Morrison microphysics are used for the reference ensemble member (Table 1). The long-wave radiation scheme is RRTMG for all ensemble members. The NOAH-MP switches are the same for all ensemble members, including the vegetation option, the stomatal resistance (Ball-Berry), the surface layer drag coefficient (Monin-Obukhov), and the radiative transfer option.

In order to investigate the effects of the different parameterization involved systematically, the schemes were changed individually. On the one hand, this choice reduced the number of total schemes included and potentially a lower spread is achieved. On the other hand, it allowed for a separation of the effects due to every single perturbation. Hence, it became possible to assess the configuration choice responsible for the largest contribution to model uncertainty. Combining the four physics with the four boundary perturbation yields in total 16 members, listed in Table 2.

2.2 | Validation datasets

Surface observations available for the Horn of Africa are not suitable to validate a model with a resolution of some kilometres, due to the lack of a dense weather station network. Only Ethiopia has a good infrastructure, including about 1,200 rain gauges and 200 high-quality weather stations (Berhanu *et al.*, 2016). However, the number of stations is in steady decline since the 1990s, they suffer from gaps in time series and the network is unevenly distributed (Dinku *et al.*, 2014; Berhanu *et al.*, 2016). The station network alone is not sufficient to provide a reference dataset with the suitable spatial resolution.

Therefore, the only alternative is the 2-m temperature provided by ECMWF operational analyses (cycles 43r3, and 45r1 from 5/06/2018; retrieved 5/11/19). They provide hourly values of atmospheric variables at about 10 km resolution. Even at a resolution coarser than WRF,

Name	LBC	PHYS	Name	LBC	PHYS
Std0	0	MOR,RRTG,MYNN	CAM0	0	MOR,CAM,MYNN
Std1	1	MOR,RRTG,MYNN	CAM1	1	MOR,CAM,MYNN
Std2	2	MOR,RRTG,MYNN	CAM2	2	MOR,CAM,MYNN
Std3	3	MOR,RRTG,MYNN	CAM3	3	MOR,CAM,MYNN
Thom0	0	THOM,RRTMG,MYNN	YSU0	0	MOR,RRTMG,YSU
Thom1	1	THOM,RRTMG,MYNN	YSU1	1	MOR,RRTMG,YSU
Thom2	2	THOM,RRTMG,MYNN	YSU2	2	MOR,RRTMG,YSU
Thom3	3	THOM,RRTMG,MYNN	YSU3	3	MOR,RRTMG,YSU

TABLE 2 Summary of the 16 members of the WRF ensemble

this is the best gridded dataset available. However, we must take into account that analyses are not equivalent to measurements since they are the result of data assimilation and thus a model run. A small number of weather stations, for which NMA provided complete time series, was used for point-like comparisons to assess the bias of analysis and model temperature in different parts of the model domain. Temperature data sets (both analysis and WRF output) were interpolated to the SEAS5 resolution using the bilinear interpolation method provided by the Earth System Modelling Framework package included in the Ncar Command Language (NCL, 2019).

Satellite-based measurements are available for precipitation with good spatial resolution. Considering the requirements on spatial resolution (order of few km), time period and temporal frequency, the global precipitation mission - integrated multi-satellite retrieval for GPM (GPM-IMERG) V06B Half-Hourly Precipitation Final Run ([Huffman *et al.*, 2019] retrieved on 05/08/2019) was the best choice to validate precipitation among the available data sets at the time of writing, notwithstanding their known uncertainties and limitations, that is, conditional bias (Xu *et al.*, 2016). The GPM-IMERG V06B half-hourly early run is produced using only satellite observations but the research-level product is adjusted to produce a monthly accumulation equal to the monthly Final Run. This bias calibration is based on gauge measurements, namely the monthly product by the Global Precipitation Climatology Centre precipitation data set. GPM-IMERG spatial resolution is 0.1° with coverage from 60°S to 60°N . The Climate Hazards Group InfraRed Precipitation with Station data (CHIRPS) is obtained by merging satellite Cold Cloud Duration measurements and gauges. The final research-level product is available at 0.05° resolution in pentads and monthly accumulation, while daily values are only available as a preliminary product. More details can be found in (Funk *et al.*, 2015). In order to show the relative uncertainty in observations, the seasonal accumulated values of GPM-IMERG and CHIRPS were considered, but only the former was used for further model evaluation. The GPM-IMERG grid is the reference

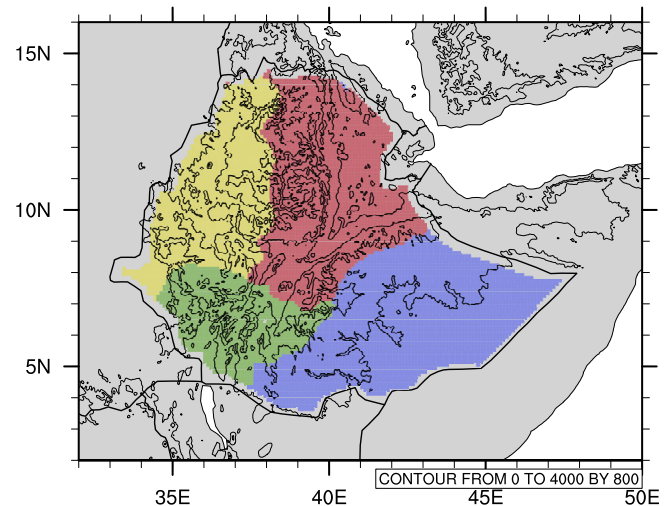


FIGURE 2 Ethiopia is partitioned in four clusters, based on climatic and precipitation patterns. In blue the Somali region (cluster 1), in green the South-West (cluster 2), in yellow the Western highlands (cluster 3) and in red the Afar region (cluster 4). Black curves show WRF model elevation, 0–4,000 m by 800 [Colour figure can be viewed at wileyonlinelibrary.com]

used to compare the precipitation data sets to take advantage of its high resolution: the SEAS5 model output is disaggregated using the nearest-neighbour method while the WRF output is regridded using bilinear interpolation.

2.3 | Partition of Ethiopia in homogeneous sub-regions for the analysis

The model domain included diverse climates due to the high mountains influencing temperatures, wind patterns and rainy seasons' timing, duration and accumulated values. As Ethiopian highlands are the region receiving most of the precipitation during summer in East Africa, the analyses focused on this area. Ethiopia was partitioned into four regions identified using Principal Component Analysis and the k-means clustering method on monthly mean precipitation amounts with results similar to Nikulin *et al.* (2018). The clusters are depicted in Figure 2.

FIGURE 3 Temperature and precipitation climatology of the four Ethiopian sub-regions. The red lines represent the mean monthly temperature ($^{\circ}\text{C}$), the blue bars the monthly total precipitation (mm) [Colour figure can be viewed at wileyonlinelibrary.com]

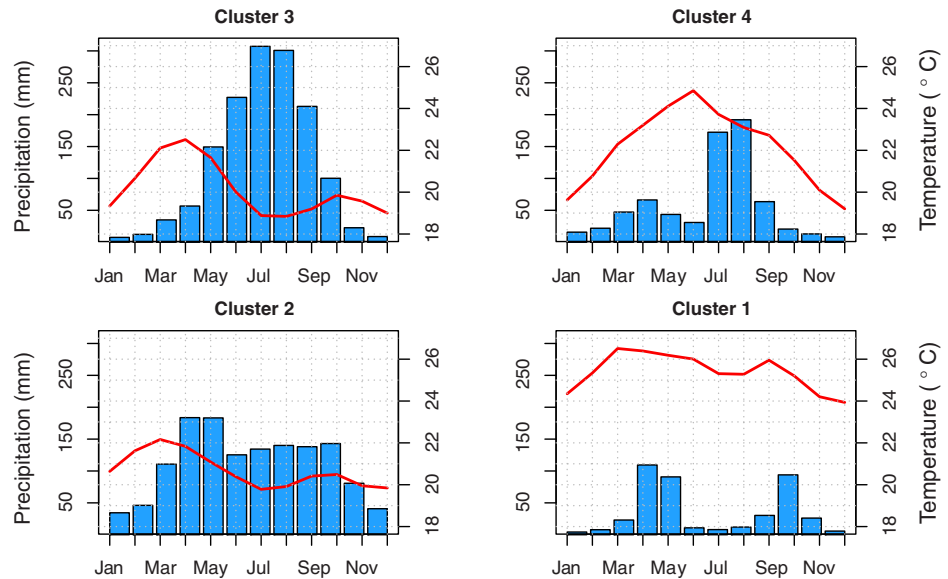


Figure 3 shows their climatology (1985–2018), using CHIRPS for precipitation and CRU (Harris *et al.*, 2014) for temperature. Spatially averaged temperature has a weak annual cycle, in the range of 2°C , in southern Ethiopia. Clusters 3 and 4 show stronger seasonal variations: 3 and 6°C respectively. The hottest periods are registered just before the beginning of the rainy season. Precipitation patterns are more articulated:

1. South Eastern Ethiopia, the Somali region, is dry during summer. It has a well-defined bi-modal distribution of precipitation: long (MAM) and short (ON) rainy seasons when large-scale conditions allow the moisture to flow in from the Indian Ocean to transform into rainfall.
2. The South Western highlands have a constant temperature and abundant precipitation from March to October: the long rainy season (MAM) is followed by less intense precipitation during summer and autumn.
3. The Western mountains are most influenced by the West-African monsoon (WAM): during the summer moist air is advected in by the low-level westerly winds. The orographic lifting triggers convection and then intensifies precipitation from June to September. The overall precipitation distribution is unimodal, with maximum in July and August.
4. In the north-east lies a lowland area, the Afar region, encircled by some of the highest mountain peaks. Intense precipitation and storms hit the mountains during mid-to-late summer generating a unimodal precipitation distribution with peak in August. The low Afar area remains in the rain shadow.

3 | RESULTS

In this work, we focus on T2m and accumulated precipitation as the main variables of interest in a seasonal forecast.

3.1 | Temperature

Figure 4 shows the mean summer temperature of 2018 ECMWF analysis, SEAS5 four-member ensemble forecast and 16-member WRF ensemble. Due to the limited resolution of the archived SEAS5 data, the mean temperature in Figures 4 and 5 was calculated as the average of values at 00:00 and 12:00 UTC. The model biases are calculated with respect to the ECMWF analysis. The SEAS5 forecast (Figure 4d) reveals a 1°C bias over most of the Horn of Africa, mainly east of the Rift Valley. Lowlands in Northern Ethiopia are subject to a cold bias of about 2°C and the Ethiopian highlands and the area to their west are well represented. The WRF ensemble mean (Figure 4e) has a stronger warm bias in the Somali region and at the border between Ethiopia and Kenya but the intensity decreases approaching the Indian Ocean coastline. The cold bias in the northern coastline is reduced while a warm bias is seen in the Gulf of Aden and some parts of Yemen. A 2°C warm bias is instead produced in the northwestern part of the domain, near the Ethiopia-Sudan border. On average, the Ethiopian mountains have a slightly higher temperature than in the analysis. In Table 3 the seasonal T2m average of a selected group of weather stations is compared to analysis and model averages. Weather stations in south Ethiopia (Moyale, Burji) prove that both models are warmer than measurements, with WRF showing a larger bias than SEAS5. A similar situation occurs in the western part of the domain: the measurements in Khartoum, Gimbi, and Dangala confirm the WRF warm bias in the area, larger than 2°C compared to the station measurements, which are close to the analysis. However, the SEAS5 temperature is comparable to WRF in Gimbi and Dangala but colder in Khartoum, which closer to observations. In the north-east

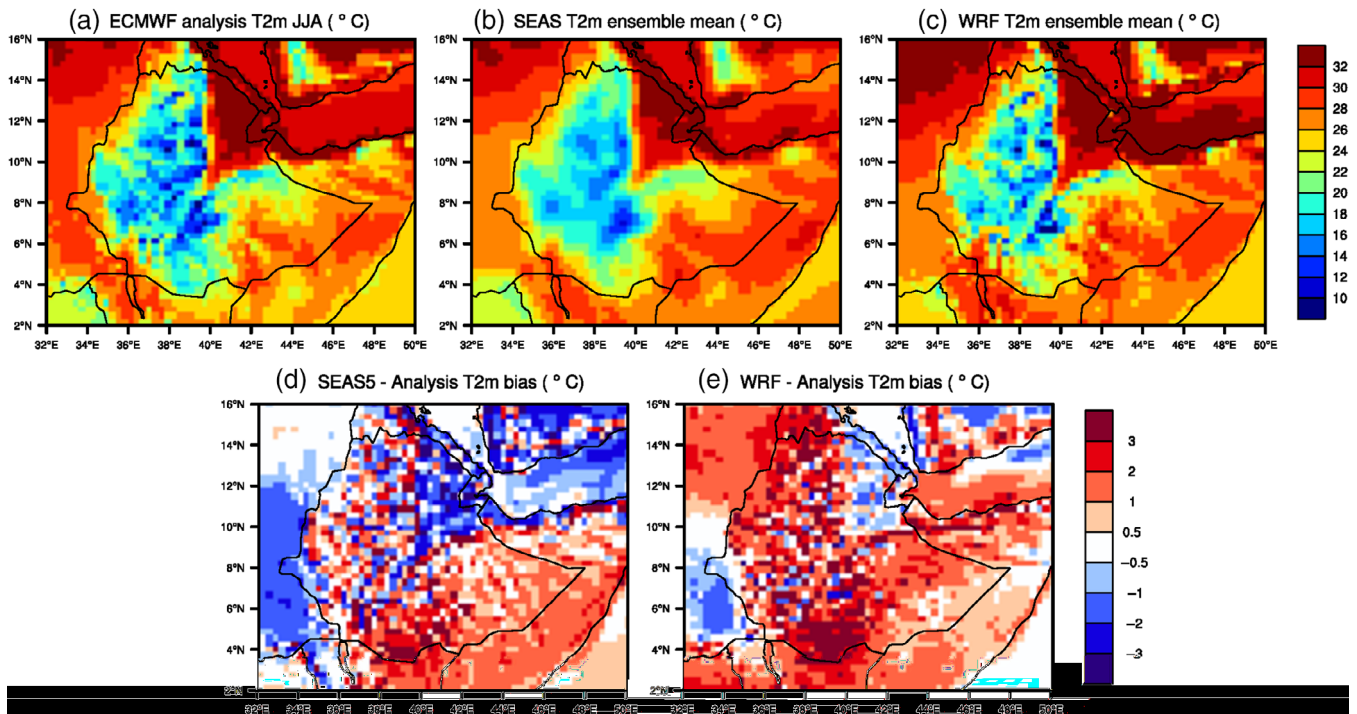


FIGURE 4 Mean JJA 2 m temperature for (a) ECMWF analysis T2m JJA ($^{\circ}\text{C}$), (b) the SEAS5 T2m ensemble mean ($^{\circ}\text{C}$), and (c) the WRF T2m ensemble mean ($^{\circ}\text{C}$). Model temperature biases are calculated with respect to the analysis: (d) SEAS5 - analysis T2m bias ($^{\circ}\text{C}$) and (e) WRF - analysis T2m bias ($^{\circ}\text{C}$). The bias for the study area is 0.17°C for SEAS5 and 1.14°C for WRF, which is 0.65% and 4.3% warmer, respectively [Colour figure can be viewed at wileyonlinelibrary.com]

plain (Dalli Fage), the WRF T2m is very close to the observation and the analysis, while SEAS5 suffers a cold bias. In the highlands the situation is more complex, given the sharp changes in elevations: SEAS5 and analysis have lower mean T2m than the measurements in both stations (Ambo, Weliso). The WRF warm bias in this area is therefore overestimated when compared to the analysis rather than the observations. Average summer temperature for the four regions is displayed in Table 3. The results for Ethiopia show a split between the southern and the northern half: in the south, WRF follows the SEAS5 output, yielding warmer temperatures than the analysis (Table 3). In the northern half the SEAS5 forecast is much better than WRF. The GCM forecast has no bias, whereas the WRF ensemble has $+1^{\circ}\text{C}$ bias in north-west Ethiopia and almost $+2^{\circ}\text{C}$ in the north-eastern quadrant (Table 3).

All WRF ensemble members are displayed in Figure 5: in order to make the inter-ensemble variations easier to visualize and link to the member perturbation, the ensemble mean, instead of observations, is taken as reference. Depending on model physics, fluctuations in the 2°C range are visible on the south-eastern portion of the Horn of Africa. The same bias is seldom reached elsewhere: most members do not exceed a 1°C bias. Crucially, only two members, namely CAM0 (Figure 5c) and YSU0 (Figure 5d), have a significantly reduced warm bias in

Sudan (or cold bias with respect to the ensemble-mean). The impact of LBCs is evident only when comparing the control member with the perturbed ones: Ethiopian highlands are generally warmer (up to 1°C with respect to the ensemble mean) while the Horn tip is about 0.5°C colder in the perturbed runs.

3.2 | Precipitation

GPM-IMERG and CHIRPS accumulated precipitation are shown in Figure 6a,b, respectively. The large scale distributions are in good agreement, meaning that any of the two can be used as reference without affecting the results in the following. However, there are some differences: CHIRPS has more homogeneous north-south distribution over the Ethiopian highlands but differs from GPM which displays larger accumulated values in excess of 1,200 mm in the northern area. Compared to GPM, the accumulated precipitation predicted by the SEAS5 JJA (Figure 6c) mean is larger over the southern part of the Ethiopian highlands, with a generally good match in spatial distribution due to the presence of orographic forcing. The WRF ensemble mean (Figure 6d) has very high precipitation totals in the vicinity and to the west of the highest peak in the region. Similarly to the parent model,

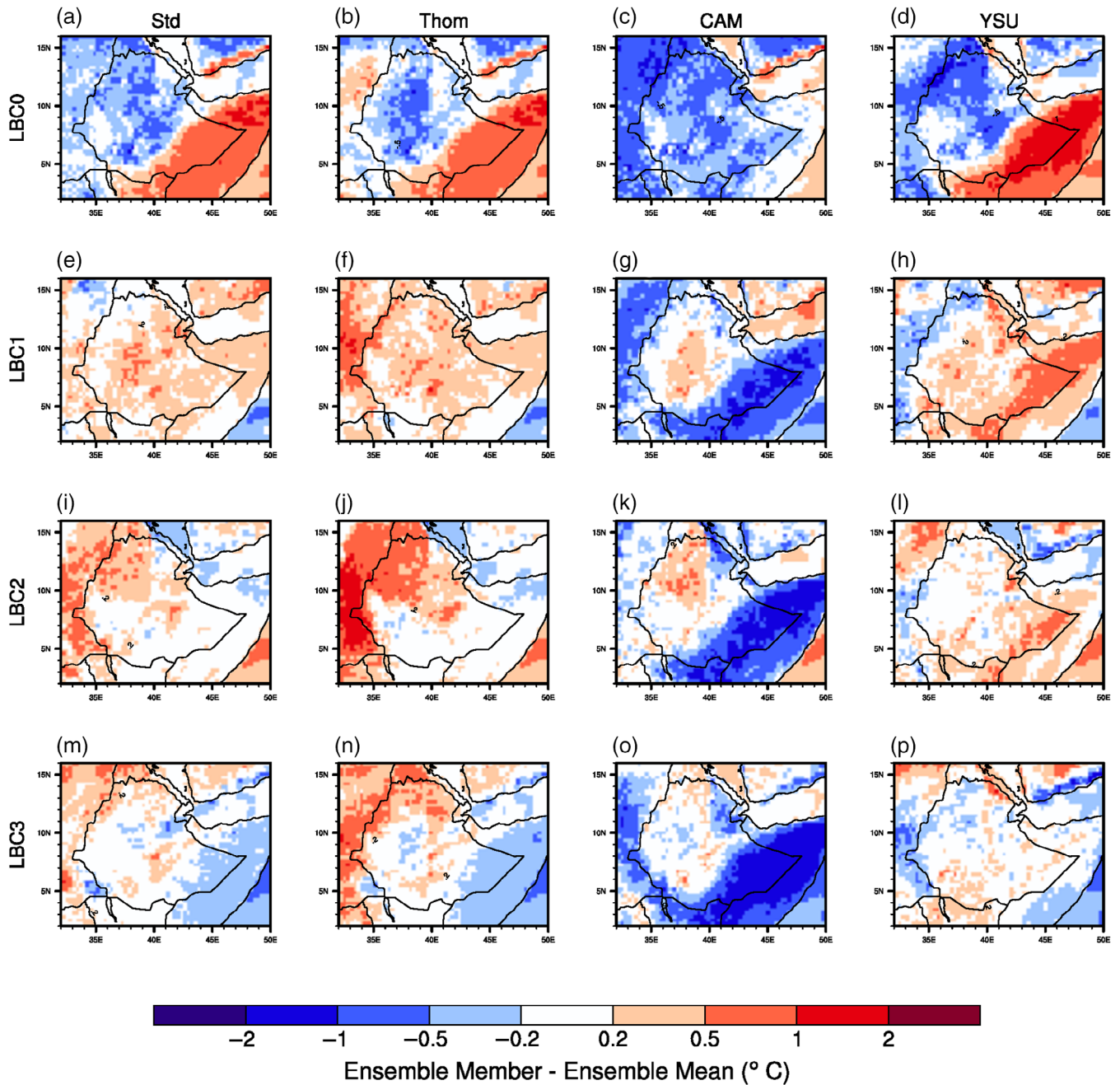


FIGURE 5 2 m temperature bias of individual WRF ensemble members with respect to the WRF ensemble mean. Boundary conditions (LBC) perturbation are arranged in rows, with the control in the top row. Physics perturbations are organized in columns, with the control (Std.) to the left [Colour figure can be viewed at wileyonlinelibrary.com]

TABLE 3 Cluster averaged mean 2 m temperature in summer 2018 \pm SD

	ECMWF analysis ($^{\circ}$ C)	SEAS5 mean ($^{\circ}$ C)	WRF mean ($^{\circ}$ C)
Somali	24.5	26.2 \pm 0.6	26.3 \pm 0.5
South	18.3	19.2 \pm 0.2	19.9 \pm 0.2
West	19.8	20.2 \pm 0.2	21.6 \pm 0.3
North	23.3	23.0 \pm 0.3	24.4 \pm 0.3

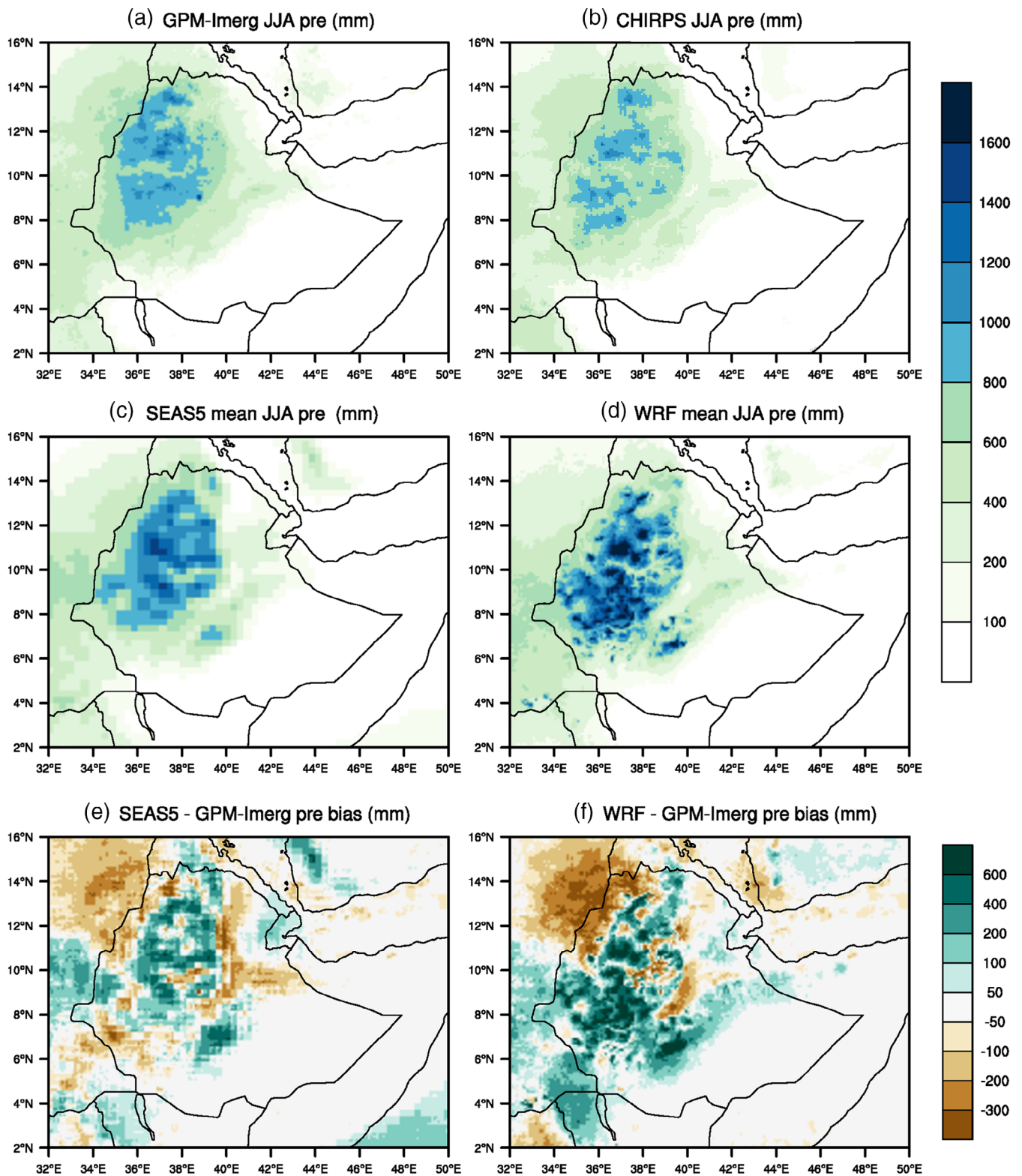


FIGURE 6 Accumulated JJA precipitation for (a) GPM-IMERG JJA pre (mm), (b) CHIRPS JJA pre (mm), (c) the SEAS5 ensemble mean JJA pre (mm), and (d) the WRF ensemble mean JJA pre (mm). Model bias is calculated with respect to the GPM-IMERG observation: (e) SEAS5 - GPM-IMERG pre bias (mm) and (f) WRF - GPM-IMERG pre bias (mm). The bias over the study area is 12.28 mm for SEAS5 and 28.10 mm for WRF, which means 5.2% and 11.9% wetter compared to GPM-IMERG, respectively [Colour figure can be viewed at wileyonlinelibrary.com]

the wet bias is larger over the southern part of the highlands than in the northern half, but the WRF accumulated values are significantly higher. A dry bias is present in the northwestern part of the domain for both SEAS5 and WRF (Figure 6e,f), but in the latter case a bigger area at the foot of the Ethiopian highlands is affected. Depending on the cluster considered, a maximum of four ensemble members have a large wet bias (Figure 7a,b,d,p), of which only one does not come from the control (LBC0) boundary conditions: the downscaling does not change the drier/wetter trends of forcing members.

3.2.1 | Number of wet days

As precipitation intensity is generally subject to significant variations between models or on the interannual time-scale, the number of wet days (defined as number of days with precipitation larger than 1 mm) provides additional and less noisy information about seasonal precipitation patterns (Moron *et al.*, 2006; Moron *et al.*, 2007). Figure 8 shows that Sudan and nearby areas see a shorter precipitation period in the WRF downscaling with respect to the observations. The eastern part of the Rift Valley is instead subject to a longer wet period. Concerning the SEAS5

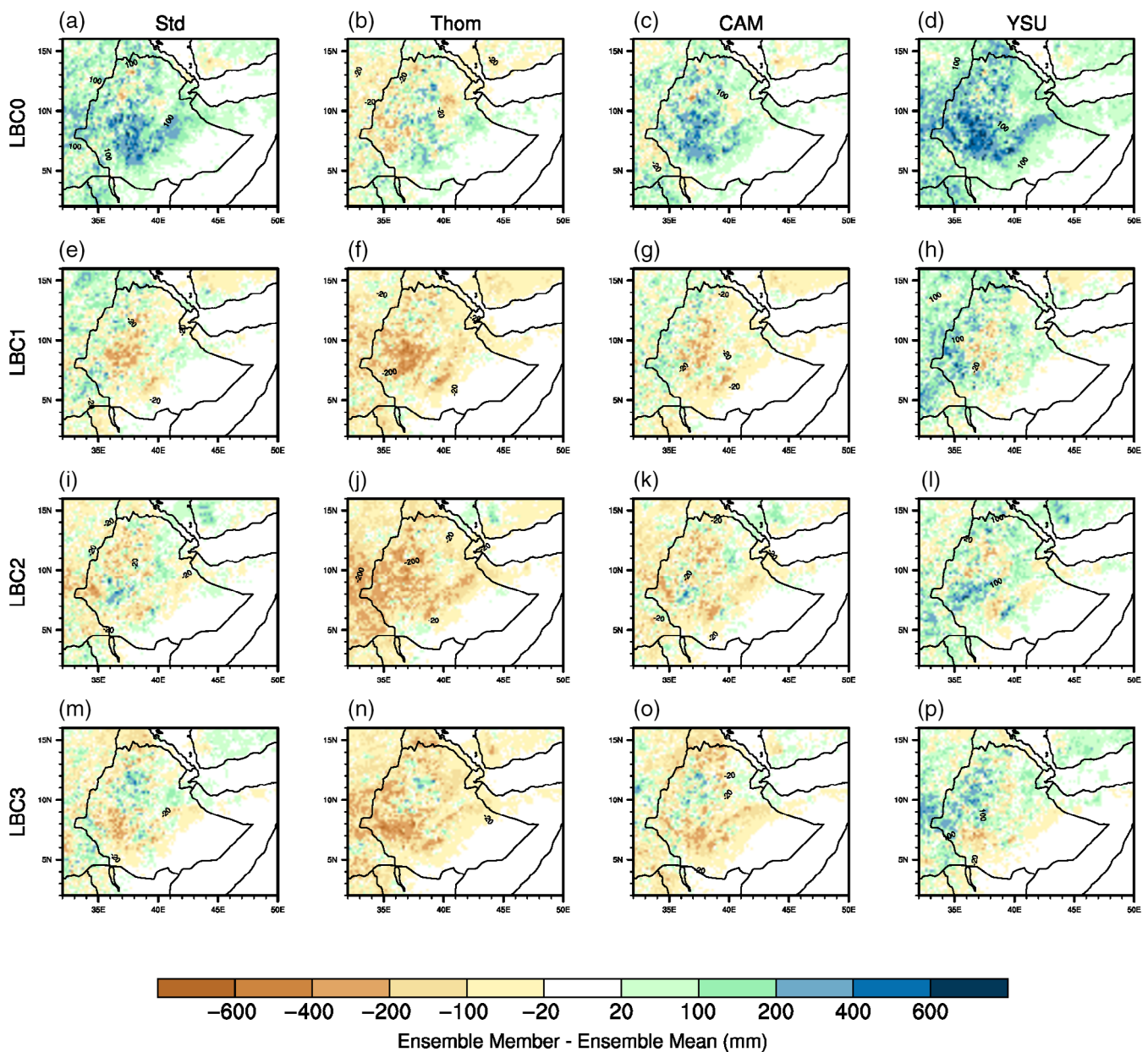


FIGURE 7 Same as in Figure 5, but for total precipitation [Colour figure can be viewed at wileyonlinelibrary.com]

forecast, the very limited spatial variability over the highlands and the overestimation of wet days over southern Ethiopia is apparent. The global model is, however, well-tuned to produce a proper total amount of precipitation.

3.2.2 | Rain belt movement and extension

To assess whether the rain belt movement in the WRF ensemble is guided by the boundary conditions or the LAM has the capacity to significantly change its pattern, we compared IMERG, SEAS5, and WRF ensemble mean of zonally averaged (35–40°E) precipitation over time in Figure 9. (See Appendix S1 for more details on model circulation.) The LAM closely follows the large-scale circulation movement

imposed by the global model: the center of the rain belt is stationary at about 10–11°. On the contrary, observations measure a movement up to 13°N in July and August. In addition, the rain belt cover in the north is reduced: the 1 mm·day⁻¹ running average exceeds 19°N in the observation, reaches 18°N in the WRF ensemble and 17.5°N in SEAS5. The 3 mm·day⁻¹ line, which is a better indicator of useful rainfall amount (Lélé and Lamb, 2010), remains about 1° to the south of the 1 mm·day⁻¹ threshold for GPM and SEAS5, 2° to the south for WRF. However, the WRF ensemble remains at the maximum latitude for longer in late July and early August, similarly to the GPM reference. It is important to note that the comparison to previous years' GPM measurements reveals an unusual deviation of the rain belt to the north in 2018 compared to the climatological mean (not shown) (Table 4).

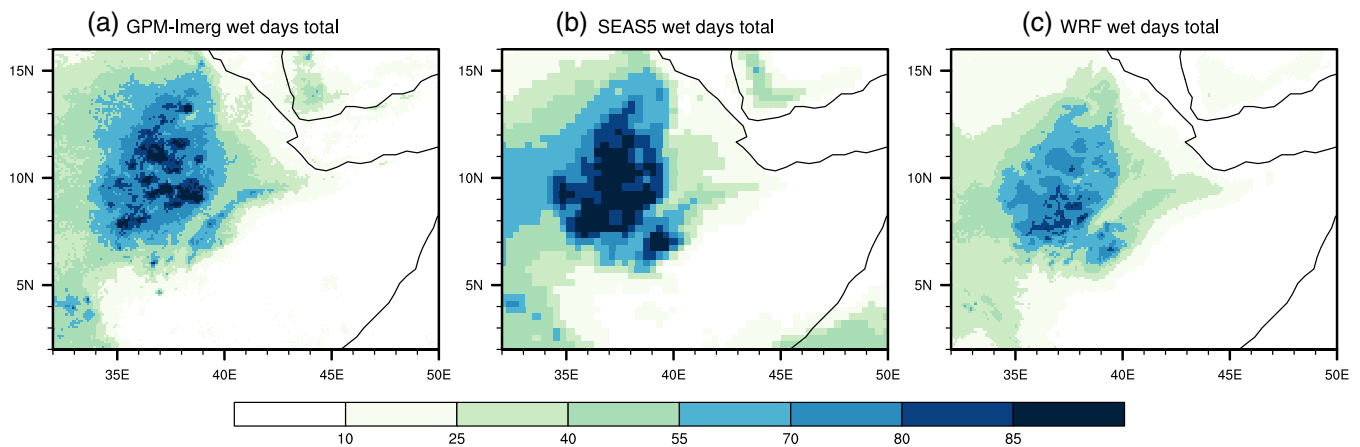


FIGURE 8 Number of wet days (precipitation·day⁻¹ > 1 mm) during June–July–August 2018. The total number of days in the season is 92. (Left) GPM-IMERG observations, (Centre) SEAS5 ensemble mean, and (Right) WRF ensemble mean [Colour figure can be viewed at wileyonlinelibrary.com]

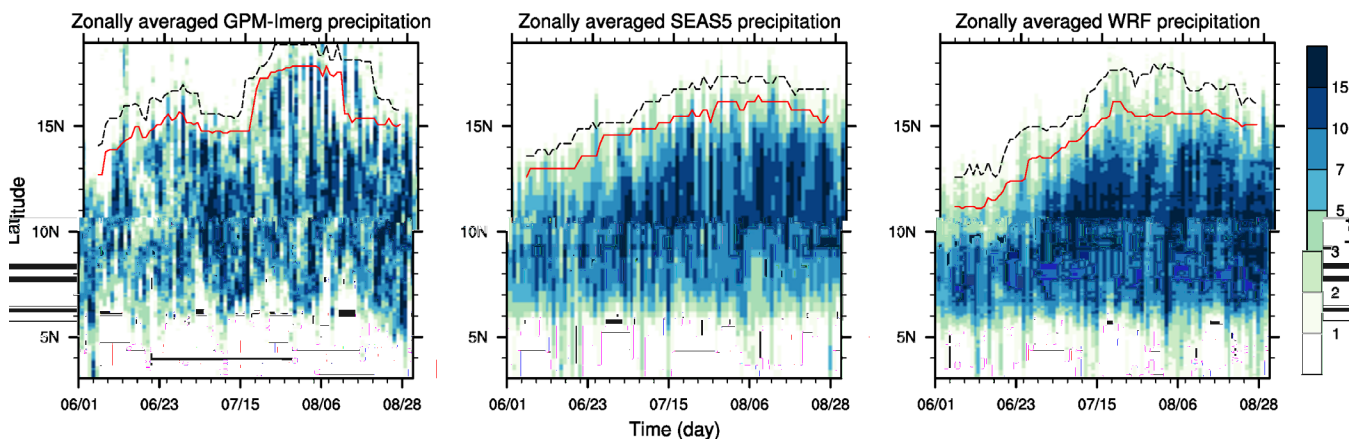


FIGURE 9 Hovmoeller plots of meridional movement of the rain belt from the 01/06 to 31/08, averaged over the Ethiopian highlands (35°E–40°E). (Left) GPM-IMERG, (Centre) SEAS5 mean, and (Right) WRF mean. Colours indicate daily precipitation intensity (mm·day⁻¹). The black line shows the northern limit of the rain belt, defined by the 1 mm·day⁻¹ value in a 10-day running average; the red line marks the 3.5 mm·day⁻¹ threshold [Colour figure can be viewed at wileyonlinelibrary.com]

TABLE 4 JJA average of T2m for weather stations, ECMWF analysis, SEAS5 mean and WRF mean

Station location	Lat (°N)	Lon (°E)	Station T2 mean (°C)	Analysis T2 mean (°C)	SEAS5 T2 mean (°C)	WRF T2 mean (°C)
Moyale	3.55	39.03	20.8	20.9	24.76 ± 0.07	24.0 ± 0.6
Burji	5.08	37.85	18.1	20.9	20.9 ± 0.5	23.4 ± 0.3
Gimbi	9.17	35.78	18.1	17.8	19.9 ± 0.1	19.9 ± 1.0
Ambo	8.98	37.83	17.2	14.6	15.7 ± 0.2	9.0 ± 1.4
Weliso	8.55	37.97	17.5	16.6	15.2 ± 0.1	18.6 ± 1.3
Dangala	11.25	36.85	16.9	16.0	18.0 ± 0.6	18.7 ± 1.2
Dalli Fage	11.81	40.19	32.1	32.0	31.0 ± 0.3	31.8 ± 0.4
Karthoum	15.59	32.55	33.3	33.3	32.26 ± 0.04	36.0 ± 0.5

Note: SD is included for SEAS5 and WRF ensembles. Due to the limitation in the SEAS5 data sets, daily mean is always calculated as mean of values at 00 and 12 UTC.

TABLE 5 Same as Table 3, for precipitation

	GPM-IMERG (mm)	SEAS5 mean (mm)	WRF mean (mm)
Somali	31.6	40 ± 12	60 ± 20
South	402	420 ± 40	680 ± 130
West	844	950 ± 60	1,000 ± 120
North	475	500 ± 40	530 ± 70

TABLE 6 Same as Table 3, for total number of wet days (pre > 1 mm·day⁻¹)

	GMP IMERG (n days)	SEAS5 mean (n days)	WRF mean (n days)
Somali	5	10 ± 2	8 ± 3
South	46	56 ± 5	52 ± 5
West	77	79 ± 4	63 ± 5
North	54	54 ± 4	45 ± 5

To summarize, precipitation patterns in the north and in the south clusters have opposite behaviours: to the south the global model overestimates the number of wet days but it produces a correct amount of rainfall (Table 5), while the downscaling is able to correctly reduce the number of wet days to match observations (Table 6). The WRF ensemble mean is however always overestimating precipitation intensity, leading to a wet bias there. North of 8°, SEAS5 matches the average number of rainy days (Table 6) because of the slightly displaced rain belt. For the same reason, WRF largely underestimates wet days but it is closer to the reference in total precipitation amount (Table 5).

3.3 | Ensemble spread

3.3.1 | Reliability differences in temperature and precipitation

An ensemble is considered to be reliable when the spread matches the mean error. Combined with the relatively large temperature biases found for the WRF ensemble mean, the

LAM limited spread does not improve ensemble reliability. As revealed in Figure 10, the ensemble spread does not vary in time and does not match the ensemble-mean error fluctuations. The SEAS5 ensemble does not show larger spread, but the mean error is generally lower, in particular in clusters 3 and 4, thus providing a better match to the ensemble spread. Concerning precipitation, the ensemble extracted from the SEAS5 forecast is under-dispersed in all clusters (Figure 11). On the contrary, the WRF ensemble variability is comparable to the ensemble-mean error in all cases, with the spread growing enough to account for the model errors when necessary. On average over Ethiopia, the spread is 70% larger in the WRF ensemble compared to SEAS5. The full SEAS5 ensemble reliability might be higher, but testing on the 10 available members did not reveal any differences with respect to the four-members reduced ensemble (not shown).

3.3.2 | Effects of lateral boundaries and physics schemes

This ensemble forecast allows to evaluate the different contributions to the ensemble spread of physics

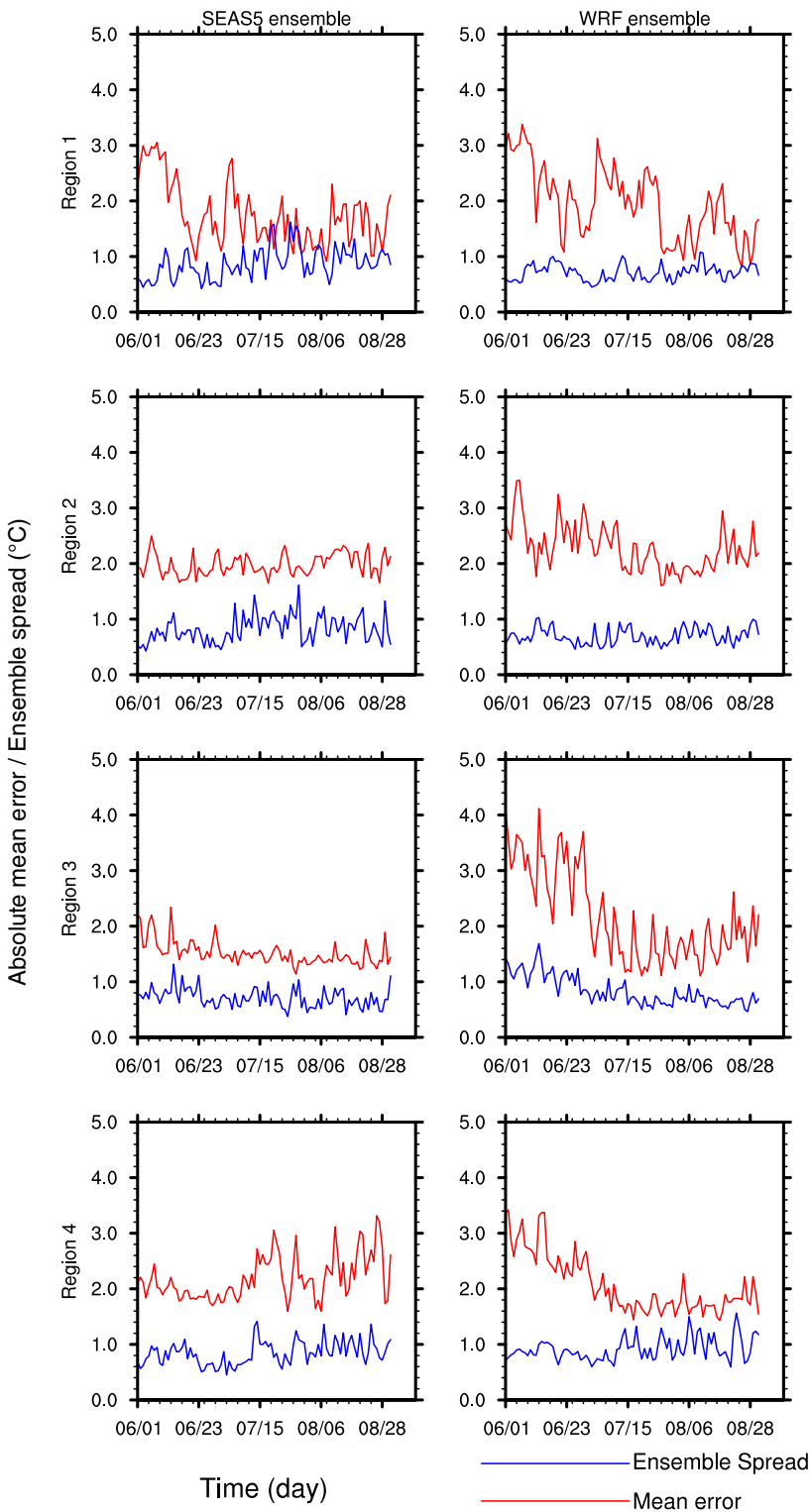


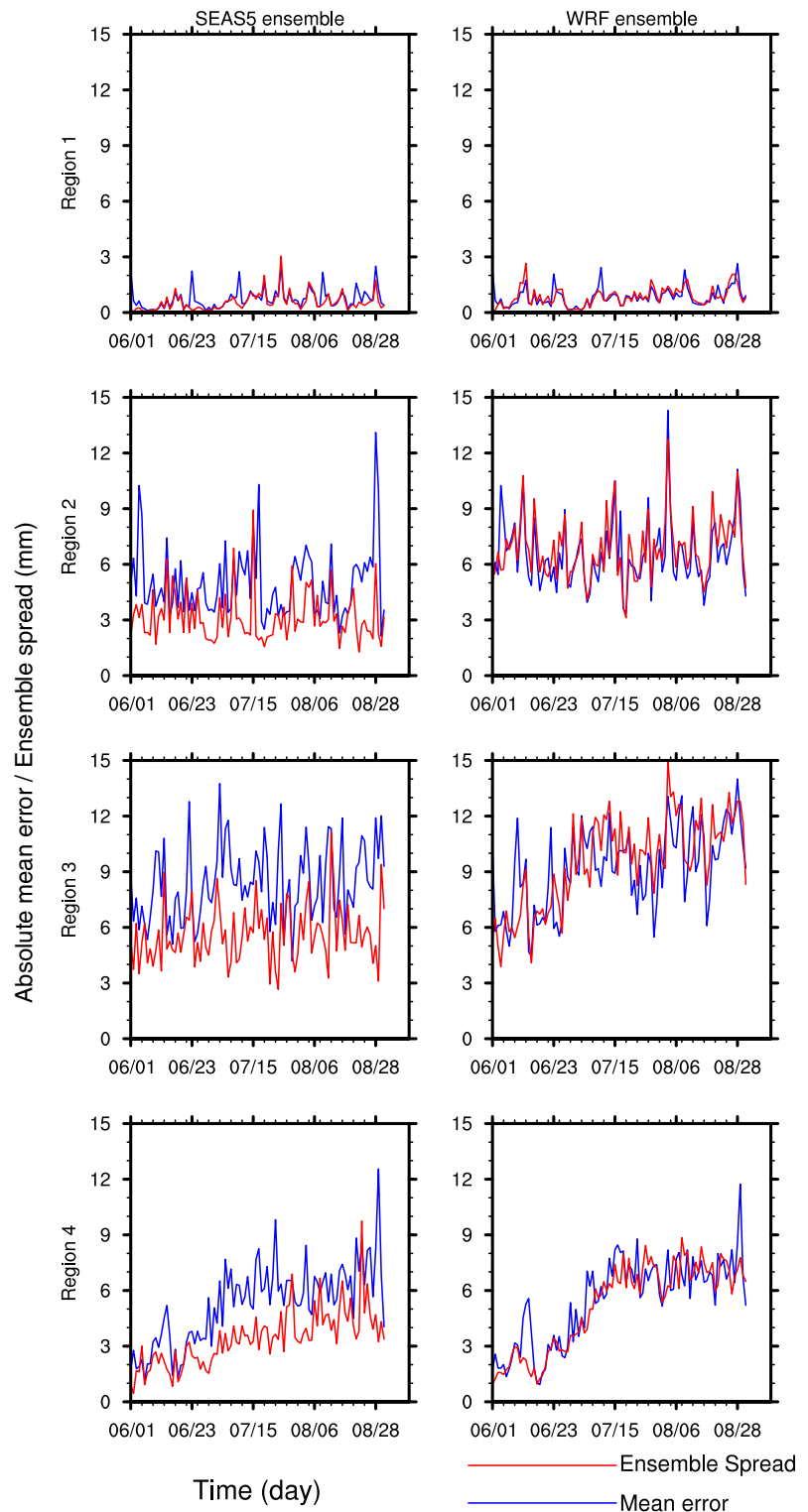
FIGURE 10 Comparison of 2 m temperature ensemble spread and mean error for each of the four Ethiopian clusters. Ensemble spread is the mean distance between each member and the ensemble mean, mean error is the distance between ensemble mean and observations. An ensemble is considered to be reliable when the spread matches the mean error. The left side displays the SEAS5 four-member ensemble, the right side the 16-member WRF ensemble [Colour figure can be viewed at wileyonlinelibrary.com]

parameterization and boundary conditions perturbations. For short, when boundary properties are concerned, the terms “LBC” spread or variability are used. Likewise, when the physics schemes are considered we refer to “PHYS”. This spread is the average value of the root mean square difference (rmsd) of sub-ensembles

constituted by ensemble members with one rotated component, that is, {std0, std1, std2, std3}, as in (Klein *et al.*, 2015).

Figure 12 shows the spatial distribution of the ensemble spread components. Model physics variations lead to a larger temperature spread in the Somali

FIGURE 11 As Figure 10, but for precipitation
[Colour figure can be viewed at
wileyonlinelibrary.com]



region, southern Ethiopia and South Sudan. Over the Ethiopian highlands, though, the lateral boundary conditions are the major source of variability. A similar pattern appears for precipitation: the model physics is responsible for larger spread over flat regions part or near to the Sahel, the Somalian coast, the Afar region of Ethiopia and part of Yemen coastline. In general, LBC spread is larger than PHYS, being

dominant over the highlands in Ethiopia and the Arabic peninsula and the Indian Ocean. Concerning the four clusters, LBCs are responsible for most of the precipitation-related uncertainty in the Ethiopian mountainous region. Western foothills are an exception: PHYS spread is locally higher, resulting in a similar averaged spread contribution from LBC and PHYS in cluster 3.

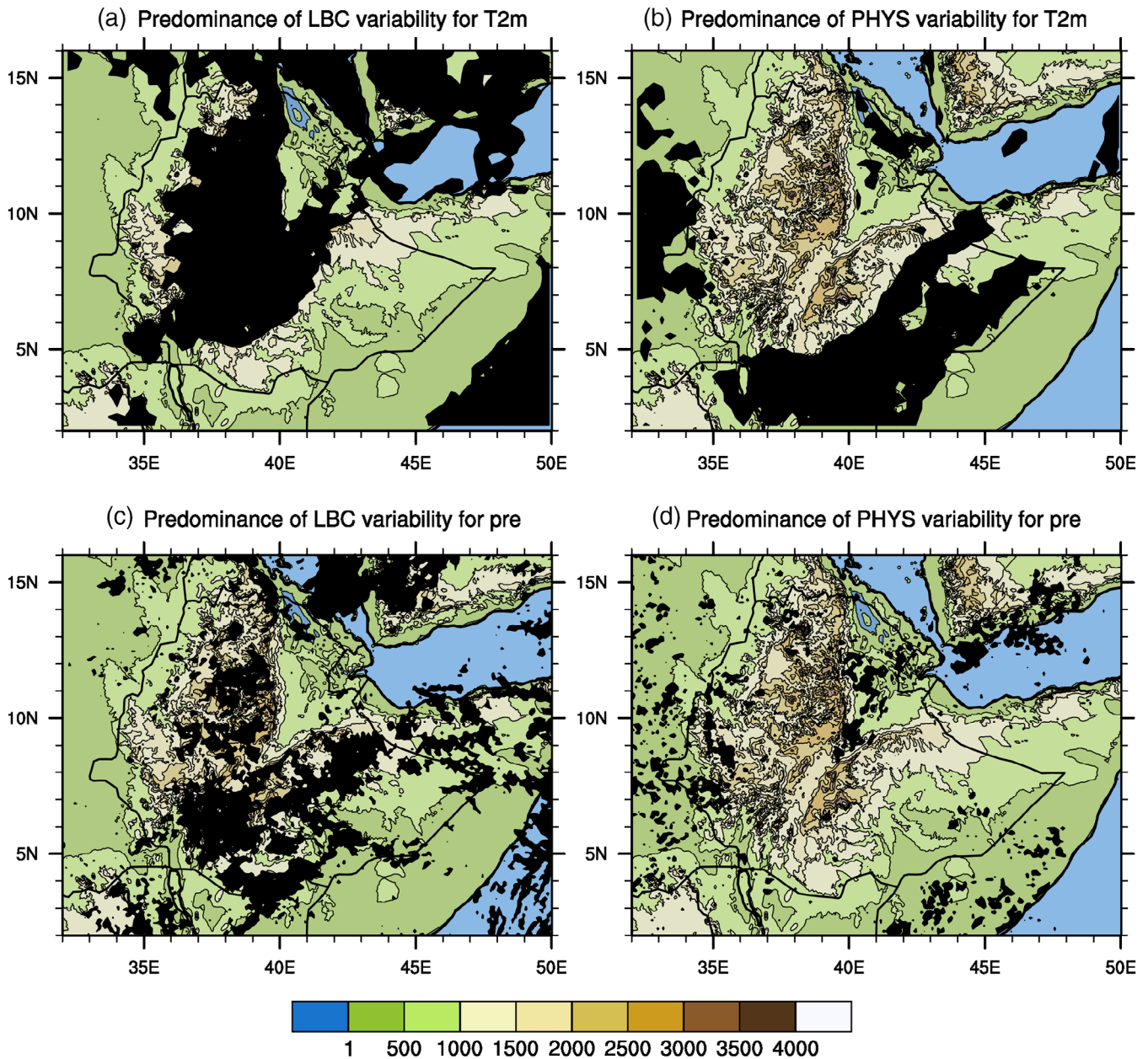


FIGURE 12 Masked areas show where the given source of variability is at least 50% larger than the other. The top row shows the results for temperature, the bottom row for precipitation. %Colour contours show the model elevation, 0–4,000 m by 500 m. (a) Predominance of LBC variability for T2m; (b) Predominance of PHYS variability for T2m; (c) Predominance of LBC variability for pre; (d) Predominance of PHYS variability for pre [Colour figure can be viewed at wileyonlinelibrary.com]

When considering the influence of single physics parameterizations, the variation of PBL, MP and SW radiation schemes produce variability patterns which are not significantly different from each other (not shown). In terms of bias, the SW radiation scheme is responsible for the largest impact on T2m. In Ethiopia, 2-m temperature is on average 0.38°C colder when CAM substitutes RRTMG. Both the microphysics and the PBL scheme changes lead to very small average differences, 0.05 and -0.005°C , respectively. For precipitation, a change in microphysics leads to the largest difference, with

$29\text{ mm}\cdot\text{month}^{-1}$ on average over Ethiopia, the Morrison scheme being wetter than Thompson. MYNN is $19\text{ mm}\cdot\text{month}^{-1}$ drier than YSU, while the SW radiation schemes are the closest at $7\text{ mm}\cdot\text{month}^{-1}$ (RRTMG wetter than CAM).

4 | DISCUSSION

The results have shown that the T2m and precipitation bias present in the GCM is not reduced by downscaling

using the current experimental setup. The sign of the bias is the same of the GCM model, but the intensity is generally higher. A known weak point in mesoscale models is the lack of a proper microphysics scheme for convection-permitting scale. The wet model bias is found in many other studies and it can be related to the parameters calibration not suitable for the resolution (Hong and Kanamitsu, 2014). Even if the WRF ensemble mean shows a wet and warm tendency, a few ensemble members agree much better with observations. It should be possible to identify model schemes to downscale SEAS5 forecasts with lower biases through a sensitivity study.

At the same time, improvements in satellite-based observation datasets are also crucial for areas where an extended network of reliable rain gauges is missing. The limited spatial and temporal resolution of many products, together with the documented conditional biases, put strong limitations to model verification at the kilometre scale, where convection-permitting models have the largest improvement potential. In addition to the general tendency, it is useful to compare Figures 5 and 7 in order to understand the effects of perturbations on the LAM. T2m of individual WRF members is displayed in Figure 5: the large T2m change in Somalia, up to 2°C (compare Figure 5c, g, k, o with the plots in the respective lines) can be attributed to the change in short-wave radiation scheme from RRTMG to CAM in dry areas, like Somalia and Sudan. We find no effect of this type for the Ethiopian highlands, and also precipitation-wise the change in SW parameterization is not very impactful in the WRF ensemble (Figure 7), contrary to what previously found (Pohl *et al.*, 2011). The substitution of the microphysics scheme has much stronger consequences on rainfall: the Thompson scheme results in a significantly drier summer (Figure 7b,f,j,n compared to maps in the same lines) in agreement with (Heikenfeld *et al.*, 2019).

Although less strong, a T2m modification due to the change from Morrison to Thompson is apparent over Sudan, South-Sudan and Eritrea (Figure 5b,f,j,n): it seems that the difference in moisture leads to higher temperature in these areas over the entire season.

Considering the PBL scheme, YSU tends to produce a dipole when compared to MYNN (Figure 5d,h,l,p): colder on the western side and warmer on the eastern one. The effect is however less pronounced than the other physics parameterization changes.

Precipitation-wise, YSU leads to increased precipitation and number of wet days (not shown), especially on the western and northern sides of the domain. The changes could be explained by differences in mixing layer moisture content, which tends to be wetter for YSU (Hariprasad *et al.*, 2014) while keeping a similar boundary layer height.

It is worth noting that the PBL parameterization has a remarkable influence on the precipitation amount in the CP model even at the seasonal scale. In fact, the SW parameterization has a strong influence on T2m but a weaker impact on rainfall than the PBL scheme. As only two SW schemes have been used in this study, the generalization is limited.

Analysing boundary conditions, large-scale regular patterns are not common. However, one clear change is apparent: the WRF members forced by the control run (SEAS5 member 0) are substantially different compared to the members with a similar physics configuration (Figures 5a–d and 7a–d compared with the respective columns), whereas the three perturbed runs are much more alike. The LBC0 runs have a strong warm bias in Somalia and eastern Ethiopia, and generally a larger excess of rainfall with respect to other WRF runs.

Concerning the ensemble dispersion, downscaling improves the under-dispersive precipitation global ensemble. Although the WRF ensemble-mean error is slightly larger than in the global model, the ensemble spread matches the error fluctuations in all clusters of Ethiopia (Figure 11). The contribution given by lateral boundary conditions to the ensemble spread is critical to achieve the right ensemble spread for precipitation. Only few and small regions see a larger variability due to model physics: for instance the western side of the domain includes part of the Sahel (Figure 12d), a region where strong land-surface feedback is expected to influence the atmosphere enough to partially control rainfall. The Horn of Africa sees a widespread prevalence of boundary conditions influence (Figure 12a,c), with the only exception being the Afar region and the Somali coast. These are very dry areas in summer, thus not a main focus for seasonal forecasters. Even if increased reliability does not actually mean that additional information is provided, a more robust probabilistic forecast would nonetheless benefit the users.

We can conclude that physics parameterization is less relevant where orographic lifting is the main trigger: moisture transport is decisive in determining whether the right conditions for precipitation occur. Therefore wind intensity and direction are crucial. Given that the exact location of precipitation is also influenced by the winds, it is not surprising that the lateral boundary conditions have such a large influence in rainfall variability. Additional material on how perturbations influence model circulation is included in Appendix S2.

The rain belt movement simulated by the WRF ensemble is similar to the global model forecast, except for minor details (Figure 9). This is in contrast with the results in (Siegmund *et al.*, 2015), where the rain belt in the limited area model did not behave correctly in mid to late summer in West Africa. Although no definitive

explanation for the problem was given in that work, it was concluded that changes in model physics would modify the model dynamics as demonstrated in (Klein *et al.*, 2015). In our experiment, model physics did not account for relevant modifications in the rain-belt pattern (as can be deduced by Figures S5–S7).

The northern extension of the WRF ensemble rain belt is slightly improved, as it reaches farther north than in the GCM during July and August. However, on the Ethiopian foothills and in Sudan there is a significant lack of precipitation in WRF in June during the monsoon onset, causing a warm and dry bias in the area. Since WRF largely underestimates the number of wet days, the lack of cloud cover and moisture, concentrated mainly in June, amplify the warm bias. In the following months, July and August, the GCM and LAM ensembles show a very similar behaviour even when mediated by the influence of topography at different resolutions. This means that boundary conditions strongly guide the rain-belt characteristics. Potential errors in the large-scale circulation in SEAS5 are carried into the CP model, where the internal model variability does not substantially deviate from the forcing. The high-resolution model might not be able to improve the forecasts. In fact, in this case it responds poorly to the imperfect boundary conditions.

WRF model climatology would be necessary to calibrate the model output to assess whether downscaling actually improves or degrades the skill of a probabilistic seasonal forecast. Thus, to draw significant conclusions on actual forecast skills achieved by downscaling, several years of hindcasts are needed and that is beyond the purpose of this research project.

5 | CONCLUSIONS AND OUTLOOK

We have presented the experimental design and the initial results of the dynamical downscaling of SEAS5 global seasonal forecasts using WRF at the CP scale. The main goal was to understand the model capability to improve simulations over the Horn of Africa and the model variability related to physics schemes and boundary conditions.

The WRF ensemble reveals that perturbed boundary conditions are necessary to achieve the right ensemble spread over the Ethiopian highlands where most of the summer rains in the Horn of Africa take place. Although model physics is generally less effective in producing ensemble spread, it has an important role in the western and southern part of the domain, where it largely affects temperature variability. Our suggestion to optimize computational resources for any forecast downscaling effort in Ethiopia or a similar mountainous region is to set up a single-physics (or single model) ensemble with a large

number of perturbed LBCs. This is also advantageous in general because hindcasts for only one model configuration would be needed, limiting overall computational costs. It should be noted that we included only perturbation of atmospheric physics and did not consider any effects related to the land-surface model, land use, and other known sources of model uncertainties. This could be the subject of further research.

Further analyses on the added value provided by the forecast downscaling are ongoing: the precipitation distribution at the grid scale can be investigated to measure the models' performance and the influence of resolution on the variable distribution and its extreme values. Benefits of downscaling can also be assessed identifying temporal and spatial scales at which added variability over the GCM model is provided, for instance by means of the potential added value score.


To complement this study, ECMWF SEAS5 or another suitable ensemble seasonal forecast (or hindcast) could be downscaled over the Colorado Basins. Downscaling of reanalysis to the CP scale has shown strong improvement in precipitation bias at the seasonal scale, thus it is an ideal spot to investigate whether the potential skill is transferred to actual forecasts. At the same time, it would allow for testing our findings on the necessity of boundary conditions perturbations.

ACKNOWLEDGEMENTS

The authors would like to thank the referees for their valuable comments and input which helped to improve the manuscript. The simulations were performed on the national supercomputer Cray XC40 at the High Performance Computing Center Stuttgart (HLRS) under the grant number WRFSFHOA/ACID 44111. The authors thank the ECMWF for providing the operational analysis data and the weather station observations in Khartoum, and the Ethiopian National Meteorology Agency for providing the additional weather stations measurements. The financial support of the “Water–People–Agriculture” Research Training Group funded by the Anton & Petra Ehrmann-Stiftung is gratefully acknowledged.

ORCID

Paolo Mori  <https://orcid.org/0000-0002-2093-3153>

Thomas Schwitalla  <https://orcid.org/0000-0002-7898-8499>

Markos Budusa Ware  <https://orcid.org/0000-0002-2310-8511>

Kirsten Warrach-Sagi  <https://orcid.org/0000-0003-2572-8527>

Volker Wulfmeyer  <https://orcid.org/0000-0003-4882-2524>

ENDNOTE

The name consists of the alternative physics scheme and the number of the boundary condition

REFERENCES

- Antic, S., Laprise, R., Denis, B. and de elía, R. (2004) Testing the downscaling ability of a one-way nested regional climate model in regions of complex topography. *Climate Dynamics*, 23(5), 473–493. <https://doi.org/10.1007/s00382-004-0438-5>.
- Argent, R., Sun, X., Semazzi, F., Xie, L. and Liu, B. (2015) The development of a customization framework for the WRF model over the Lake Victoria basin, eastern Africa on seasonal time-scales. *Advances in Meteorology*, 2015, 1–15. <https://doi.org/10.1155/2015/653473>.
- Batté, L. and Déqué, M. (2011) Seasonal predictions of precipitation over Africa using coupled ocean-atmosphere general circulation models: skill of the ENSEMBLES project multimodel ensemble forecasts. *Tellus, Series A: Dynamic Meteorology and Oceanography*, 63(2), 283–299. <https://doi.org/10.1111/j.1600-0870.2010.00493.x>.
- Berhanu, B., Seleshi, Y., Demisse, S.S. and Melesse, A.M. (2016) Bias correction and characterization of climate forecast system re-analysis daily precipitation in Ethiopia using fuzzy overlay. *Meteorological Applications*, 23(2), 230–243. <https://doi.org/10.1002/met.1549>.
- Castro, C.L., Chang, H.I., Dominguez, F., Carrillo, C., Schemm, J.K. and Henry Juang, H.M. (2012) Can a regional climate model improve the ability to forecast the North American monsoon? *Journal of Climate*, 25(23), 8212–8237. <https://doi.org/10.1175/JCLI-D-11-00441.1>.
- Cheneka, B.R., et al. (2016) Searching for an added value of precipitation in downscaled seasonal hindcasts over East Africa: COSMO-CLM Forced by MPI-ESM. *Advances in Meteorology*, 2016, 1–17. <https://doi.org/10.1155/2016/4348285>.
- Cohen, J. and Entekhabi, D. (1999) Corrections to “Eurasian snow cover variability and Northern Hemisphere climate predictability”. *Geophysical Research Letters*, 26(8), 1051. <https://doi.org/10.1029/1999GL900200>.
- Collins, W. D. et al. (2004) ‘Description of the NCAR Community atmosphere model (CAM 3.0)’, *Ncar technical note*, TN-464+STR(June), p. 214.
- Denis, B., Laprise, R. and Caya, D. (2003) Sensitivity of a regional climate model to the resolution of the lateral boundary conditions. *Climate Dynamics*, 20, 107–126. <https://doi.org/10.1007/s00382-002-0264-6>.
- Diez, E., et al. (2011) Downscaling ECMWF seasonal precipitation forecasts in Europe using the RCA model. *Tellus, Series A: Dynamic Meteorology and Oceanography*, 63(4), 757–762. <https://doi.org/10.1111/j.1600-0870.2011.00523.x>.
- Dinku, T., Hailemariam, K., Maidment, R., Tarnavsky, E. and Connor, S. (2014) Combined use of satellite estimates and rain gauge observations to generate high-quality historical rainfall time series over Ethiopia. *International Journal of Climatology*, 34(7), 2489–2504. <https://doi.org/10.1002/joc.3855>.
- Diro, G.T. (2016) Skill and economic benefits of dynamical downscaling of ECMWF ENSEMBLE seasonal forecast over southern Africa with RegCM4. *International Journal of Climatology*, 36(2), 675–688. <https://doi.org/10.1002/joc.4375>.
- Diro, G.T., Tompkins, A.M. and Bi, X. (2012) Dynamical downscaling of ECMWF ensemble seasonal forecasts over East Africa with RegCM3. *Journal of Geophysical Research Atmospheres*, 117(16), 1–20. <https://doi.org/10.1029/2011JD016997>.
- Endris, H.S., Omondi, P., Jain, S., Lennard, C., Hewitson, B., Chang’a, L., Awange, J.L., Dosio, A., Ketiem, P., Nikulin, G., Panitz, H.J., Büchner, M., Stordal, F. and Tazalika, L. (2013) Assessment of the performance of CORDEX regional climate models in simulating East African rainfall. *Journal of Climate*, 26(21), 8453–8475. <https://doi.org/10.1175/JCLI-D-12-00708.1>.
- Fekadu, K. (2015) Ethiopian seasonal rainfall variability and prediction using canonical correlation analysis (CCA). *Earth Science*, 4(3), 112. <https://doi.org/10.11648/j.earth.20150403.14>.
- Feldman, D.L. and Ingram, H.M. (2009) Making science useful to decision makers: climate forecasts, water management, and knowledge networks. *Weather, Climate, and Society*, 1(1), 9–21. <https://doi.org/10.1175/2009WCAS1007.1>.
- Funk, C., Peterson, P., Landsfeld, M., Pedreros, D., Verdin, J., Shukla, S., Husak, G., Rowland, J., Harrison, L., Hoell, A. and Michaelsen, J. (2015) The climate hazards infrared precipitation with stations - a new environmental record for monitoring extremes. *Scientific Data*, 2, 1–21. <https://doi.org/10.1038/sdata.2015.66>.
- Gleixner, S., et al. (2017) The El Niño effect on Ethiopian summer rainfall. *Climate Dynamics*, 49(5–6), 1865–1883. <https://doi.org/10.1007/s00382-016-3421-z>.
- Hariprasad, K.B.R.R., et al. (2014) Numerical simulation and intercomparison of boundary layer structure with different PBL schemes in WRF using experimental observations at a tropical site. *Atmospheric Research*, 145–146, 27–44. <https://doi.org/10.1016/j.atmosres.2014.03.023>.
- Harris, I., Jones, P.D., Osborn, T.J. and Lister, D.H. (2014) Updated high-resolution grids of monthly climatic observations - the CRU TS3.10 dataset. *International Journal of Climatology*, 34(3), 623–642. <https://doi.org/10.1002/joc.3711>.
- Heikenfeld, M., White, B., Labbouz, L. and Stier, P. (2019) Aerosol effects on deep convection: the propagation of aerosol perturbations through convective cloud microphysics. *Atmospheric Chemistry and Physics*, 19(4), 2601–2627. <https://doi.org/10.5194/acp-19-2601-2019>.
- Hong, S.Y. and Kanamitsu, M. (2014) Dynamical downscaling: fundamental issues from an NWP point of view and recommendations. *Asia-Pacific Journal of Atmospheric Sciences*, 50(1), 83–104. <https://doi.org/10.1007/s13143-014-0029-2>.
- Hong, S.-Y., Noh, Y. and Dudhia, J. (2006) A new vertical diffusion package with an explicit treatment of entrainment processes. *Monthly Weather Review*, 134(9), 2318–2341. <https://doi.org/10.1175/MWR3199.1>.
- Huffman, G.J., Stocker, E.F., Bolvin, D.T., Nelkin, E.J. and T, J. (2019) *GPM IMERG Final Precipitation L3 Half Hourly 0.1 degree x 0.1 degree V06*. Greenbelt, MD: *Goddard Earth Sciences Data and Information Services Center (GES DISC)*. <https://doi.org/10.5067/GPM/IMERG/3B-HH/06>.
- Iacono, M.J., et al. (2008) Radiative forcing by long-lived greenhouse gases: calculations with the AER radiative transfer models. *Journal of Geophysical Research Atmospheres*, 113(13), 1–8. <https://doi.org/10.1029/2008JD009944>.
- Johnson, S.J., Stockdale, T.N., Ferranti, L., Balmaseda, M.A., Molteni, F., Magnusson, L., Tietsche, S., Decremmer, D.,

- Weisheimer, A., Balsamo, G., Keeley, S.P.E., Mogensen, K., Zuo, H. and Monge-Sanz, B.M. (2019) SEAS5: the new ECMWF seasonal forecast system. *Geoscientific Model Development*, 12 (3), 1087–1117. <https://doi.org/10.5194/gmd-12-1087-2019>.
- Kerandi, N.M., Laux, P., Arnault, J. and Kunstmann, H. (2017) Performance of the WRF model to simulate the seasonal and inter-annual variability of hydrometeorological variables in East Africa: a case study for the Tana River basin in Kenya. *Theoretical and Applied Climatology*, 130(1–2), 401–418. <https://doi.org/10.1007/s00704-016-1890-y>.
- Klein, C., Heinzler, D., Bliefernicht, J. and Kunstmann, H. (2015) Variability of west African monsoon patterns generated by a WRF multi-physics ensemble. *Climate Dynamics*, 45(9–10), 2733–2755. <https://doi.org/10.1007/s00382-015-2505-5>.
- Korecha, D. and Barnston, A.G. (2007) Predictability of June–September rainfall in Ethiopia. *Monthly Weather Review*, 135 (2), 628–650. <https://doi.org/10.1175/MWR3304.1>.
- Korecha, D. and Sorteberg, A. (2013) Validation of operational seasonal rainfall forecast in Ethiopia. *Water Resources Research*, 49 (11), 7681–7697. <https://doi.org/10.1002/2013WR013760>.
- Koster, R.D., Dirmeyer, P.A., Guo, Z., Bonan, G., Chan, E., Cox, P., Gordon, C.T., Kanae, S., Kowalczyk, E., Lawrence, D., Liu, P., Lu, C.H., Malyshev, S., McAvaney, B., Mitchell, K., Mocko, D., Oki, T., Oleson, K., Pitman, A., Sud, Y.C., Taylor, C.M., Verseghy, D., Vasic, R., Xue, Y., Yamada, T. and GLACE Team. (2004) Regions of strong coupling between soil moisture and precipitation. *Science*, 305(5687), 1138–1140. <https://doi.org/10.1126/science.1100217>.
- Lauwaet, D., van Lipzig, N.P.M., van Weverberg, K., de Ridder, K. and Goyens, C. (2012) The precipitation response to the desiccation of Lake Chad. *Quarterly Journal of the Royal Meteorological Society*, 138(664), 707–719. <https://doi.org/10.1002/qj.942>.
- Lélé, M.I. and Lamb, P.J. (2010) Variability of the intertropical front (ITF) and rainfall over the West African Sudan-Sahel zone. *Journal of Climate*, 23(14), 3984–4004. <https://doi.org/10.1175/2010JCLI3277.1>.
- Maclachlan, C., et al. (2015) Global seasonal forecast system version 5 (GloSea5): a high-resolution seasonal forecast system. *Quarterly Journal of the Royal Meteorological Society*, 141(689), 1072–1084. <https://doi.org/10.1002/qj.2396>.
- Min, S.K., Zhang, X., Zwiers, F.W. and Hegerl, G.C. (2011) Human contribution to more-intense precipitation extremes. *Nature*, 470(7334), 378–381. <https://doi.org/10.1038/nature09763>.
- Moron, V., Robertson, A.W. and Ward, M.N. (2006) Seasonal predictability and spatial coherence of rainfall characteristics in the tropical setting of Senegal. *Monthly Weather Review*, 134 (11), 3248–3262. <https://doi.org/10.1175/MWR3252.1>.
- Moron, V., Robertson, A.W., Ward, M.N. and Camberlin, P. (2007) Spatial coherence of tropical rainfall at the regional scale. *Journal of Climate*, 20(21), 5244–5263. <https://doi.org/10.1175/2007JCLI1623.1>.
- Morrison, H. and Gettelman, A. (2008) A new two-moment bulk stratiform cloud microphysics scheme in the community atmosphere model, version 3 (CAM3). Part I: description and numerical tests. *Journal of Climate*, 21(15), 3642–3659. <https://doi.org/10.1175/2008JCLI2105.1>.
- Nakanishi, M. and Niino, H. (2009) Development of an improved turbulence closure model for the atmospheric boundary layer. *Journal of the Meteorological Society of Japan*, 87(5), 895–912. <https://doi.org/10.2151/jmsj.87.895>.
- NCL. (2019) NCAR Command Language (Version 6.6.2) [Software]. Boulder, Colorado: UCAR/NCAR/CISL/TDD, <http://dx.doi.org/10.5065/D6WD3XH5>.
- Nikulin, G., et al. (2018) Dynamical and statistical downscaling of a global seasonal hindcast in eastern Africa. *Climate Services*, 9 (December), 72–85. <https://doi.org/10.1016/j.cliser.2017.11.003>.
- Niu, G-Y., Yang, Z-L., Mitchell, K.E., Chen, F., Ek, M.B., Barlage, M., Kumar, A., Manning, K., Niyogi, D., Rosero, E., Tewari, M., and Xia, Y. (2011) The community Noah land surface model with multiparameterization options (Noah-MP): 1. Model description and evaluation with local-scale measurements. *Journal of Geophysical Research*, 116 (D12), <http://dx.doi.org/10.1029/2010jd015139>.
- Osima, S., Indasi, V.S., Zaroug, M., Endris, H.S., Gudoshava, M., Misiani, H.O., Nimusiima, A., Anyah, R.O., Otieno, G., Ogwang, B.A., Jain, S., Kondowe, A.L., Mwangi, E., Lennard, C., Nikulin, G. and Dosio, A. (2018) Projected climate over the Greater Horn of Africa under 1.5°C and 2°C global warming. *Environmental Research Letters*, 13(6), 1–10. <https://doi.org/10.1088/1748-9326/aaba1b>.
- Pal, S., Chang, H.I., Castro, C.L. and Dominguez, F. (2019) Credibility of convection-permitting modeling to improve seasonal precipitation forecasting in the southwestern United States. *Frontiers in Earth Science*, 7(March), 1–15. <https://doi.org/10.3389/feart.2019.00011>.
- Pohl, B., Crétat, J. and Camberlin, P. (2011) Testing WRF capability in simulating the atmospheric water cycle over Equatorial East Africa. *Climate Dynamics*, 37(7–8), 1357–1379. <https://doi.org/10.1007/s00382-011-1024-2>.
- Prein, A.F., Holland, G.J., Rasmussen, R.M., Done, J., Ikeda, K., Clark, M.P. and Liu, C.H. (2013) Importance of regional climate model grid spacing for the simulation of heavy precipitation in the Colorado headwaters. *Journal of Climate*, 26(13), 4848–4857. <https://doi.org/10.1175/JCLI-D-12-00727.1>.
- Prein, A.F., Langhans, W., Fosser, G., Ferrone, A., Ban, N., Goergen, K., Keller, M., Tölle, M., Gutjahr, O., Feser, F., Brisson, E., Kollet, S., Schmidli, J., Lipzig, N.P.M. and Leung, R. (2015) A review on regional convection-permitting climate modeling: demonstrations, prospects, and challenges. *Reviews of Geophysics*, 53(2), 323–361. <https://doi.org/10.1002/2014RG000475>.
- Regassa, B.C. (2014) WRF preliminary results simulation of JJAS precipitation over Ethiopia under different land surface models. *Journal of Ethiopian Meteorological Society*, 2 (January), 3–10.
- Schwitalla, T., Bauer, H.S., Wulfmeyer, V. and Warrach-Sagi, K. (2017) Continuous high-resolution midlatitude-belt simulations for July–August 2013 with WRF. *Geoscientific Model Development*, 10(5), 2031–2055. <https://doi.org/10.5194/gmd-10-2031-2017>.
- Schwitalla, T., Bauer, H.S., Wulfmeyer, V. and Zängl, G. (2008) Systematic errors of QPF in low-mountain regions as revealed by MM5 simulations. *Meteorologische Zeitschrift*, 17(6), 903–919. <https://doi.org/10.1127/0941-2948/2008/0338>.
- Shukla, J. (1998) Predictability in the midst of chaos: a scientific basis for climate forecasting. *Science*, 282(5389), 728–731. <https://doi.org/10.1126/science.282.5389.728>.
- Siegmund, J., Bliefernicht, J., Laux, P. and Kunstmann, H. (2015) Toward a seasonal precipitation prediction system for West

- Africa: performance of CFSv2 and high-resolution dynamical downscaling. *Journal of Geophysical Research*, 120(15), 7316–7339. <https://doi.org/10.1002/2014JD022692>.
- Skamarock, W. C. *et al.* (2008) 'A Description of the Advanced Research WRF Version 3', *Technical Report*, (June), p. 113. doi: 10.5065/D6DZ069T.
- Stockdale, T., *et al.* (2018) ECMWF's new long-range forecasting system SEAS5'. *ECMWF Newsletter*, 154(154), 15–20. <https://doi.org/10.21957/tsb6n1>.
- 'Strengthening Climate Information Partnerships - East Africa (SCIP EA)' (2019). Available at: <https://www.metoffice.gov.uk/about-us/what/working-with-other-organisations/international/projects/wiser/scipea>.
- Thompson, D.W.J., Baldwin, M.P. and Wallace, J.M. (2002) Stratospheric connection to Northern Hemisphere wintertime weather: implications for prediction. *Journal of Climate*, 15(12), 1421–1428. [https://doi.org/10.1175/1520-0442\(2002\)015<1421:SCTNHW>2.0.CO;2](https://doi.org/10.1175/1520-0442(2002)015<1421:SCTNHW>2.0.CO;2).
- Thompson, G., Field, P.R., Rasmussen, R.M. and Hall, W.D. (2008) Explicit forecasts of winter precipitation using an improved bulk microphysics scheme. Part II: implementation of a new snow parameterization. *Monthly Weather Review*, 136, 5095–5115. <https://doi.org/10.1175/2008MWR2387.1>.
- Tölle, M.H., Gutjahr, O., Busch, G. and Thiele, J.C. (2014) Increasing bioenergy production on arable land: does the regional and local climate respond? Germany as a case study. *Journal of Geophysical Research*, 119(6), 2711–2724. <https://doi.org/10.1002/2013JD020877>.
- Vitart, F. (2014) Evolution of ECMWF sub-seasonal forecast skill scores. *Quarterly Journal of the Royal Meteorological Society*, 140(683), 1889–1899. <https://doi.org/10.1002/qj.2256>.
- Xu, S., Shen, Y. and Du, Z. (2016) Tracing the source of the errors in hourly IMERG using a decomposition evaluation scheme. *Atmosphere*, 7(12), 1–12. <https://doi.org/10.3390/atmos7120161>.
- Yuan, X., Liang, X.Z. and Wood, E.F. (2012) WRF ensemble downscaling seasonal forecasts of China winter precipitation during 1982–2008. *Climate Dynamics*, 39(7–8), 2041–2058. <https://doi.org/10.1007/s00382-011-1241-8>.

SUPPORTING INFORMATION

Additional supporting information may be found online in the Supporting Information section at the end of this article.

How to cite this article: Mori P, Schwitalla T, Ware MB, Warrach-Sagi K, Wulfmeyer V. Downscaling of seasonal ensemble forecasts to the convection-permitting scale over the Horn of Africa using the WRF model. *Int J Climatol*. 2020; 1–21. <https://doi.org/10.1002/joc.6809>